TRENDS IN SCIENCES 2025; 22(12): 10466
https://doi.org/10.48048/tis.2025.10466
RESEARCH ARTICLE

In Silico Evaluation of Novel 3-Piperoylindole Compounds Synthesized from Piperine (*Piper Nigrum* Linn.) for Potential Anti-Cancer

Syaiful Bahri[1,*], Devi Nur Annisa[1], Yuli Ambarwati[1], Lina Marlina[2], Sutiarno[3], Deana Wahyuningrum[4] and Ganjar Andhulangi[5]

[1]*Department of Chemistry, Faculty of Mathematics and Science, Lampung University, Bandar Lampung 35145, Indonesia*
[2]*Department of Agribusiness, Faculty of Agriculture, Lampung University, Bandar Lampung 35145, Indonesia*
[3]*Department of Physics, Faculty of Mathematics and Science, Lampung University, Bandar Lampung 35145, Indonesia*
[4]*Department of Chemistry, Faculty of Mathematics and Natural Sciences, Bandung Institute of Technology, Bandung 40132, Indonesia*
[5]*Department of Chemistry, Faculty of Mathematics and Natural Sciences, Universitas Gadjah Mada, Yogyakarta 55281, Indonesia*

([*]Corresponding author's e-mail: syaiful.bahri@fmipa.unila.ac.id)

Received: 25 April 2025, Revised: 27 May 2025, Accepted: 7 July 2025, Published: 30 August 2025

Abstract

The development of drugs that inhibit EGFR tyrosine kinase (EGFR-TK) is necessary to improve the effectiveness and durability of cancer treatment. *In silico* study employed a molecular docking approach to simulate the interaction between 3-piperoylindole (3-PI), a novel semi-synthetic derivative of piperine (*Piper nigrum* Linn.), and EGFR-TK. Redocking between the receptor and the original ligand yielded an RMSD value of 1.382 Å. The yield of the 3-PI compound was 37% w/w from piperoic acid. The docking results revealed that 3-PI (−8.7 kcal/mol) had a higher binding affinity than erlotinib (−7.7 kcal/mol) toward EGFR-TK. The binding affinity of 3-PI toward EGFR-TK was attributed to hydrophobic interactions and hydrogen bonds. These findings highlight the potential of this compound as anti-cancer for further *in vitro* and *in vivo* evaluation.

Keywords: 3-piperoylindole, EGFR tyrosine kinase, *Piper nigrum* Linn., Anticancer, *In silico*

Introduction

Globally, cancer is one of the leading causes of morbidity and mortality. The number of new cancer cases was estimated to reach 2.1 million by 2025, with approximately 30.27% of these cases resulting in fatal outcomes [1]. Currently, chemotherapy is the most commonly used therapy. Although patients' health can recover in many cases, this therapy has highly painful side effects, including severe impairment of the immune system, damage to normal tissues, and a lack of selectivity in targeting cancer cells [2]. Several cancer drugs have been developed in research to address these challenges. However, drug resistance remains an unavoidable issue, including therapeutic resistance and cancer recurrence [3]. Therefore, understanding the critical role of the epidermal growth factor receptor (EGFR) in the signaling pathways regulating cell activity is essential.

The targeted therapy for cancer has increasingly focused on mutations in receptor tyrosine kinases, particularly the epidermal growth factor receptor (EGFR), which plays a critical role in the pathogenesis of various epithelial malignancies. Notably, EGFR-driven lung adenocarcinomas represent a major subtype of non-small cell lung cancer (NSCLC) that is responsive to first-generation EGFR inhibitors such as erlotinib and gefitinib [4]. Tyrosine kinases are critical targets due to their significant role in regulating EGFR signaling [5]. Generally, several categories of targeted

therapies are available, including EGFR antisense inhibitors [6], monoclonal antibodies [7], and tyrosine kinase inhibitors [8]. Tyrosine kinases play an important role in regulating growth factor signaling. The active form of this enzyme has the potential to promote angiogenesis and metastasis, trigger anti-apoptotic effects, and increase tumor cell proliferation and growth [9].

Activation of protein kinases by somatic mutations is a common mechanism in tumor formation, in addition to activation by growth factors. Ligand binding triggers tyrosine kinase dimerization at the receptor, leading to autophosphorylation of the cytoplasmic domain and activation of tyrosine kinase activity [10]. Proliferation, differentiation, and survival of cancer cells are facilitated by the activation of growth receptors, including the epidermal growth factor receptor (EGFR), which has a significant impact on the RAS signaling pathway, mitogen-activated protein kinase, phosphatidylinositol-3 kinase/Akt, signal transducer and activator of transcription, and phospholipase C [11]. The development of various types of cancer is associated with uncontrolled cell proliferation and metastasis [12]. Effective regulation of EGFR activity is an emerging approach in cancer therapy [13]. One of the drug developments aligned with this global approach is the utilization of bioactive compounds extracted from natural sources, particularly piperine isolated from black pepper (*Piper nigrum* Linn.), which has been modified to evaluate its bioactivity as a potential anti-cancer.

Piperine has potential bioactivity, including antioxidant [14], anti-inflammatory [15], antimicrobial [16], and anti-cancer [17]. This compound has been reported to inhibit the expression of matrix metalloproteinase-9 (MMP-9), P-glycoprotein (P-gp), cytochrome P450 3A4 (CYP3A4), and EGFR tyrosine kinase (EGFR-TK) [18]. For instance, Paarakh et al. [18] reported on an *in silico* study conducted on piperine against EGFR-TK. This compound exhibited a binding energy of −7.6 kcal mol^{-1} with two hydrogen bonds. Evaluating semi-synthetic piperine derivatives such as 3-piperoylindole (3-PI) against EGFR-TK is of interest through a molecular docking approach.

Here, we propose a synthesis route for piperine derivatives to produce 3-PI via a pre-target compound mechanism (piperoyl chloride). This synthesis route is proposed to reduce the mixture of inorganic esters as by-products that affect the integrity of the target compound and minimize reorientation. However, the development of drug resistance, particularly due to secondary mutations like T790M in EGFR-TK, remains a major clinical challenge. This mutation induces a steric hindrance that reduces the binding affinity of first-line inhibitors, necessitating the discovery of alternative ligands or next-generation inhibitors. Therefore, *in silico* approaches such as molecular docking and virtual screening are increasingly employed to identify novel small molecules that can overcome resistance and bind effectively to mutated EGFR variants.

Hence, this study aims to screen potential inhibitors from natural bioactive compounds, such as 3-PI compound against EGFR-TK mutations using molecular docking simulations. AutoDock Vina was used for docking simulations due to its balance between accuracy and computational efficiency. The present research also explores the role of ligand protonation states and docking reproducibility to ensure robustness of the computational findings.

Materials and methods

Materials

The raw material used in this study was black pepper (*Piper nigrum* Linn.). Hydrochloric acid (HCl, Merck), potassium hydroxide (KOH, Merck), thionyl chloride ($SOCl_2$, Sigma-Aldrich), anhydrous calcium chloride ($CaCl_2$, Merck), indole (C_8H_7N, Merck), ethanol (C_2H_5OH, Merck), dimethylformamide (DMF, Merck), benzene (C_6H_6, Merck), and chloroform ($CHCl_3$, Merck) were used for extraction, isolation, and synthesis.

Procedure

Sample preparation

Black pepper fruits (*Piper nigrum* Linn.) of the Natar II variety was obtained from the Spices and Medicinal Plants Research Center (Balittro) in Natar, South Lampung. This raw sample was initially dried and pulverized in a porcelain mortar.

Isolation of piperine (1) from black paper

Extraction

Piperine isolation was performed using the soxhlet method used by Bahri et al. [19]. Black pepper powder (100–500 g) was extracted with 95% ethanol (500–

1,000 mL) using the soxhlet method. The crude extract was collected and allowed to settle at room temperature.

Purification

The crude extract was filtered to obtain the filtrate. This filtrate was then left to stand for 24 h to obtain shiny yellow needle-like crystals. These crystals were obtained by vacuum filtration using a Büchner funnel, followed by washing with a certain amount of ethanol. The crystals were tested for melting point and thin-layer chromatography (TLC) to determine their purity.

Characterization

The pure crystals were then analyzed using an ultraviolet-visible spectrophotometer (UV-Vis, model 8452-A) at 200–400 nm and Fourier transform infrared spectroscopy (FTIR, PerkinElmer FTIR-800) at 400–4,000 cm^{-1}, respectively, to determine the electronic transitions of the bonds and functional groups of the compound.

Synthesis of piperic acid (2) via hydrolysis

5 g of piperine was hydrolyzed with 100 mL of 10% KOH solution in ethanol using reflux at 60 °C for 24 h. The reflux solution was then concentrated using a rotary evaporator. The resulting residue was cooled in ice water, dissolved in warm water, and acidified with 6 N HCl to pH 3. Due to the use of corrosive reagents (10% KOH and 6 N HCl), all steps involving these chemicals were performed with appropriate safety precautions, including the use of personal protective equipment and the operation of a fume hood if necessary. The precipitate obtained is recrystallized from ethanol and allowed to settle for 24 h to obtain piperic acid crystals. This crystal was then analyzed using the same instrument to determine their melting point and for structural determination. The yield of piperic acid was obtained of 1 g (0.0046 mol) to use further step.

Synthesis of 3-piperoylindole (3) via piperoyl chloride

1 g of piperic acid was dissolved in 10 mL of $CHCl_3$ in a round-bottom flask. Then, 0.4 mL of $SOCl_2$ and 5 drops of DMF (as a catalyst) were added. The mixture was refluxed in a water bath at 50 °C with vigorous stirring for 15 min. During the initial reflux, bubbles form (indicating the formation of SO_2 and HCl gases). The mixture was then refluxed further at 60 °C for 30 min until gas formation ceases. The resulting piperoyl chloride (2a) was obtained in solution and used directly in the next step.

0.01 mL of indole in benzene was prepared in a round-bottom flask. The piperoyl chloride solution (2a) (prepared in the previous step) was slowly added dropwise through a separating funnel while stirring continuously into the indole solution. After completion, the precipitate was isolated by filtration and recrystallized from $CHCl_3$ to obtain pure crystals. The crystals were tested for melting point and TLC to ensure the purity of the product, including analyzed using the same previous characterization.

In silico study: Molecular docking protocol

The 3-dimensional crystal structure of the EGFR kinase domain (EGFR-TK, PDB ID: 4HJO) was obtained from the Protein Data Bank. Autodock Vina and MGL Tools 1.5.7 software were used to calculate Gasteiger charges and add all hydrogen atoms to the 3D crystal structure of the protein. Ligands were designed and optimized using Avogadro version 1.2.0, where Gasteiger charges were assigned and protonation states were adjusted to simulate physiological pH conditions. The structures were energy-optimized using the MMFF94 force field. The ligands were made to have rotatable bonds using the “set number of torsions” and “choose torsions” functions and then saved in pdbqt format.

An 11th generation Intel® Core™ i5-1135G7 processor @2.40 GHz (8 CPU) ~2.4 GHz and 8,192 MB RAM were used to perform docking simulations on a PC running the Windows 11 Home-64-bit operating system (10.0, Build 22631). The software applications used were Autodock Vina and MGL Tools 1.5.7 for docking simulations, PyMol2 for RMSD analysis, and Biovia Discovery Studio 2021 for visualizing ligand-receptor interactions. Docking validation was performed by redocking the protein and its original ligand at the active site of the target protein, using a 40 Å cubic grid box with a distance of 0.375 Å (EGFR-TK protein). The accepted RMSD value was less than 2 (RMSD < 2). The protein EGFR-TK coordination coordinates are 24.407, 9.151, and −0.636 (x, y, and z), with a completeness value of 16. The original ligand was replaced with 3-

piperoylindole (3-PI) and erlotinib in a similar protocol, according to the size and position of the cubic grid box for each protein. Twenty poses were obtained, and interactions were visualized by selecting the pose with the lowest bond energy.

Results and discussion

Structure elucidation of compounds (1), (2), and (3)

Piperine (**1**) was successfully isolated from black pepper powder (*Piper nigrum* Linn.), yielding 6.17 g of pure piperine from 215 g of starting material (2.86% w/w). The melting point of the yellow crystals obtained was 128.5–129.5 °C [20]. **Figure 1(a)** shows the UV spectrum with maximum wavelengths (λ_{max}) at 204, 244, 256, 310, and 342 nm, centered at 342 nm [20]. Absorption at 204 nm (band K) and 244–256 nm (band B) corresponds to π→π* transitions in aromatic/heteroaromatic rings. The peak at 310 nm indicates the presence of a chromophore with 2–3 conjugated bonds, characteristic of asymmetrically substituted aromatics (range 270–350 nm). However, structural determination based solely on UV data was uncertain. Hence, FTIR analysis was required for confirmation of functional groups.

Figure 2(a) displays the FTIR spectra to identify key vibrational modes: Amide (>N–C=O) stretch at 1,635.5 cm^{-1}, Aliphatic C=C stretch at 1,581.5 cm^{-1}, -CH_2 bending at 1,442.7 cm^{-1} (and 1,100–1,400 cm^{-1} region), =C-O-C- stretches at 1,195.8 cm^{-1} and 1,249.8 cm^{-1}, Aliphatic C-H stretches (2,862.2–2,939.3 cm^{-1}), Aromatic C-H stretch at 3,008.7 cm^{-1}, Aromatic ring vibration at 1,488.9 cm^{-1}. The signals at 1,635.5, 1,581.5, 1,249.8 and 996.0 cm^{-1} are characteristic of piperine [21] corroborating the structure.

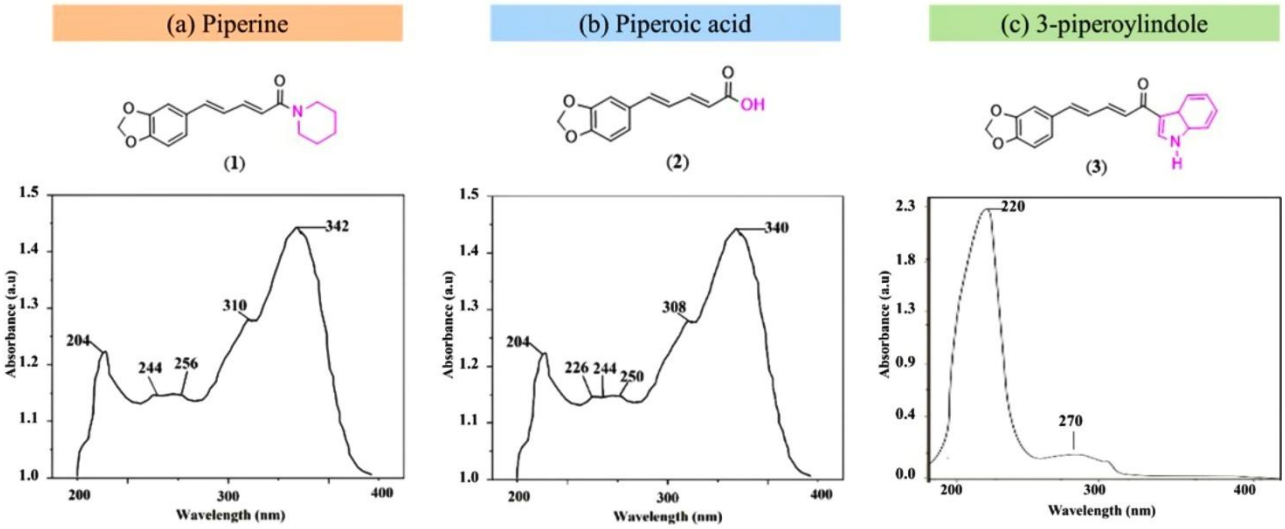

Figure 1 UV spectra of (a) piperin (**1**), (b) piperoic acid (**2**), and (c) 3-piperoylindole (**3**).

Piperoic acid (**2**) was synthesized via hydrolysis of piperine (**1**) under 100 mL of 10% KOH solution in ethanol using reflux method. Compound **2** had characteristics of smooth, needle-shaped crystals exhibiting a vivid yellow hue that is more intense than that of piperine crystals and lacks glossiness. The crystals were purified by recrystallization from hot ethanol. Based on the hydrolysis process, this product emits a pleasant aroma, which is characteristic of carboxylic acids. Based on the hydrolysis process, 3.25 g of piperoic acid was obtained, yielding 65% (w/w).

The melting point of the compound **2** was 215–216 °C [22]. **Figure 1(b)** presents the UV spectra with the maximal wavelengths (λ_{max}) of this compound were 204, 226, 244, 250, 308 and 340 nm. Although there is a modest hypsochromic shift from 334 nm (λ_{max} of piperoic acid standard), the λ_{max} of 340 nm was an indicator of piperoic acid absorption. The presence of an aromatic benzene ring was suggested by the absorbance at λ_{max} 204 nm (K-band), which was a result of the π→π* transition. The bathochromic shift of the K-band, which is indicative of the absorption of substituents in

the form of conjugated carboxyl groups and carboxylic acids, can be observed from λ_{max} 226 nm. In comparison to piperine, compound **2** exhibited a characteristic λ_{max} and endured a substantial change in UV absorption, exhibiting hypsochromic shifts at λ_{max} of 226 and 340 nm. Hence, these findings demonstrate that piperoic acid (**2**) has been succesfully synthesized so that additional validation through FTIR analysis was required.

Figure 2(b) shows the FTIR spectra to identify the substantial alteration in the bond vibrations and functional groups of compounds **2** in comparison to the preceding FTIR spectra of compound **1** (**Figure 2(a)**). Absorption changes was observed at 1,674.2 cm^{-1}, which suggests the presence of stretching vibrations of the >C=O (carboxyl group). In addition, the stretching vibration of -OH was observed to exhibit a characteristic broad band from 2,922.0 - 3,652.9 cm^{-1}. The stretching vibration of -C-O- was also detected at 1,309.6 cm^{-1} [23]. These characteristic absorptions showed the -CH_2 bending vibrations at 995.2 and 1,448.4 cm^{-1}, the =C-O-C- stretching vibrations at 1,193.0 and 1,255.6 cm^{-1}, the aromatic ring group of benzene at 1,460.0 cm^{-1}, the stretching vibration of -C=C- at 1,598.0 cm^{-1}, and the stretching vibration of -C-H aliphatic at 2,852.6 cm^{-1}, which was also suitable with UV analysis [24].

Data such as melting points, UV spectra, and FTIR spectra of each compound provide information used to propose plausible mechanisms. **Figure 3(a)** presents a proposed mechanism for the hydrolysis of piperine (**1**) to piperoic acid (**2**). Electron resonance in the carbonyl group triggers the hydrolysis of compound **1** with KOH in ethanol, producing a carbocation intermediate in the carbonyl group. This intermediate is produced when KOH interacts with the carbonyl group. The elimination step is hindered because the reaction proceeds via the release of the amine group (piperidine). To facilitate this step, hydrochloric acid (HCl) is added to protonate the amine, converting it into a better leaving group and thereby accelerating the elimination process. Compound **2** was produced by the hydrolysis process, including the by-products such as KCl and piperidine. This compound can be further used to synthesize the pre-target compound **2a** (piperoyl chloride).

The synthesis of compound **2a** as a pre-target compound was carried out through a nucleophilic substitution reaction. The reagent $SOCl_2$ was used in the synthesis of compound **2a** from compound **2**, which was obtained in the previous stage. The synthesis process using these reagents was chosen due to its various advantages, including the ability to reduce rearrangement in the reaction mechanism, resulting in a pure compound 2a. Additionally, the reaction conditions are relatively easy to operate, with a temperature of 50–60 °C for 30 min. Furthermore, these reagents are compatible with the organic solvents used in the reaction, preventing the product from undergoing hydrolysis. Under certain conditions, the combination of $SOCl_2$ with or without a catalyst can provide greater flexibility, but this will also affect the reaction rate.

Figure 3(b) shows a possible mechanism for compound **2a**. For the synthesis of this compound, compound **2** was reacted with $SOCl_2$ using a DMF catalyst in $CHCl_3$ solvent. The leaving group was released in the form of chloride ions (Cl^-) by the $SOCl_2$ reagent, which was triggered by the DMF reagent. The role of DMF was to activate $SOCl_2$ through the formation of a Vilsmeier-type complex. The acyl chlorosulfite intermediate was formed through resonance of compound **2**, which was soluble in $CHCl_3$ solvent. This compound interacts with the $SOCl_2$ ion. The reaction between the Cl^- ion and part of the carboxyl group occured in the intermediate compound. By releasing SO_2 and HCl gases, the compound undergoes rearrangement to achieve stability. The solution phase form of compound **2a** was obtained. To obtain purified compound **2a** for the synthesis of the target compound, 3-piperoylindole (**3**), the procedure for removing SO_2 and HCl gases was tested using litmus paper.

Figure 3(c) shows the possible mechanism of the pre-target compound piperoyl chloride (**2a**) resulting 3-piperoylindole (**3**). Compound **2a** was reacted with indole in benzene to synthesize compound **3**. The carbonyl group in compound **2a** resonates to form an intermediate compound. Benzene solvent was used to prevent hydrolysis. This intermediate interacts with the lone pair of electrons from the indole molecule, yielding compound **3**, followed by the release of HCl. Compound 3 was obtained as a pure red brick-colored crystal with a yield of 37% (0.37 g from 1 g of piperoic acid). The melting point of this compound was obtained at 173.5–174.2 °C, which analyzed using UV-Vis spectrophotometer and FTIR.

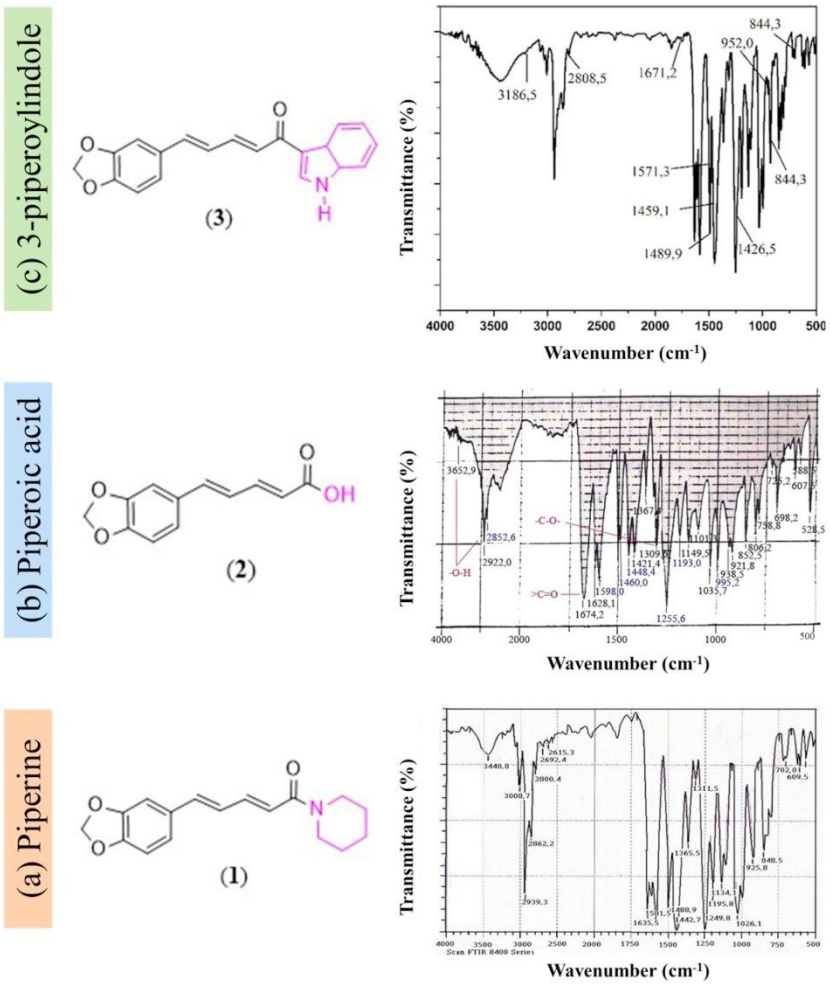

Figure 2 FTIR spectra of (a) piperin (**1**), (b) piperoic acid (**2**), and (c) 3-piperoylindole (**3**).

Figure 1(c) shows the UV spectra with maximum wavelengths (λ_{max}) of compound 3 observed at 220 and 270 nm. The absorption in the K band and B band at λ_{max} 220 and 270 nm is the result of $\pi \rightarrow \pi^*$ transitions. The carboxyl group (-COOH) in compound **2**, the indole ring in compound **3**, and the piperidine ring portion in compound **1** may contribute to the variation in characteristic λ_{max} absorption. For example, compound **1** exhibited characteristic λ_{max} absorption at 342 nm, compound **2** at 340 nm, and the target compound **3** presented λ_{max} at 220 and 270 nm. Therefore, compound **3** was then analyzed by FTIR to confirm the success of its synthesis.

Figure 3(c) shows the FTIR spectra, which indicates the characteristic absorption of 3-piperoylindole (**3**). The region at 2,808.5 cm^{-1} indicates aliphatic C-H stretching vibrations. The region at 1,571.2 cm^{-1} indicates stretching vibrations from aliphatic -C=C-. This absorption was also consistent with the signals observed in the UV spectra, indicating the presence of 2–3 aliphatic conjugated bonds. The absorption of the aromatic benzene ring is also detected at 1,489.9 cm^{-1}. The vibration of the -CH_2 and =C-O-C- groups show absorption at 1,459.1 cm^{-1} and 952.0 cm^{-1}, respectively. The bending vibration of the -CH_2 group, characteristic of piperine in the piperidine ring, is slightly reduced and appears at 1,459.1 cm^{-1}. The absorption regions at 1,671.2 cm^{-1}, 844.3 cm^{-1}, and 741.4 cm^{-1} show a significant change in signal for compound **3**, indicated as the stretching vibration and amide bond of the >N-C=O group. These absorption peaks were attributed to the stretching vibrations of the -C-O-C- group in the indole ring [19].

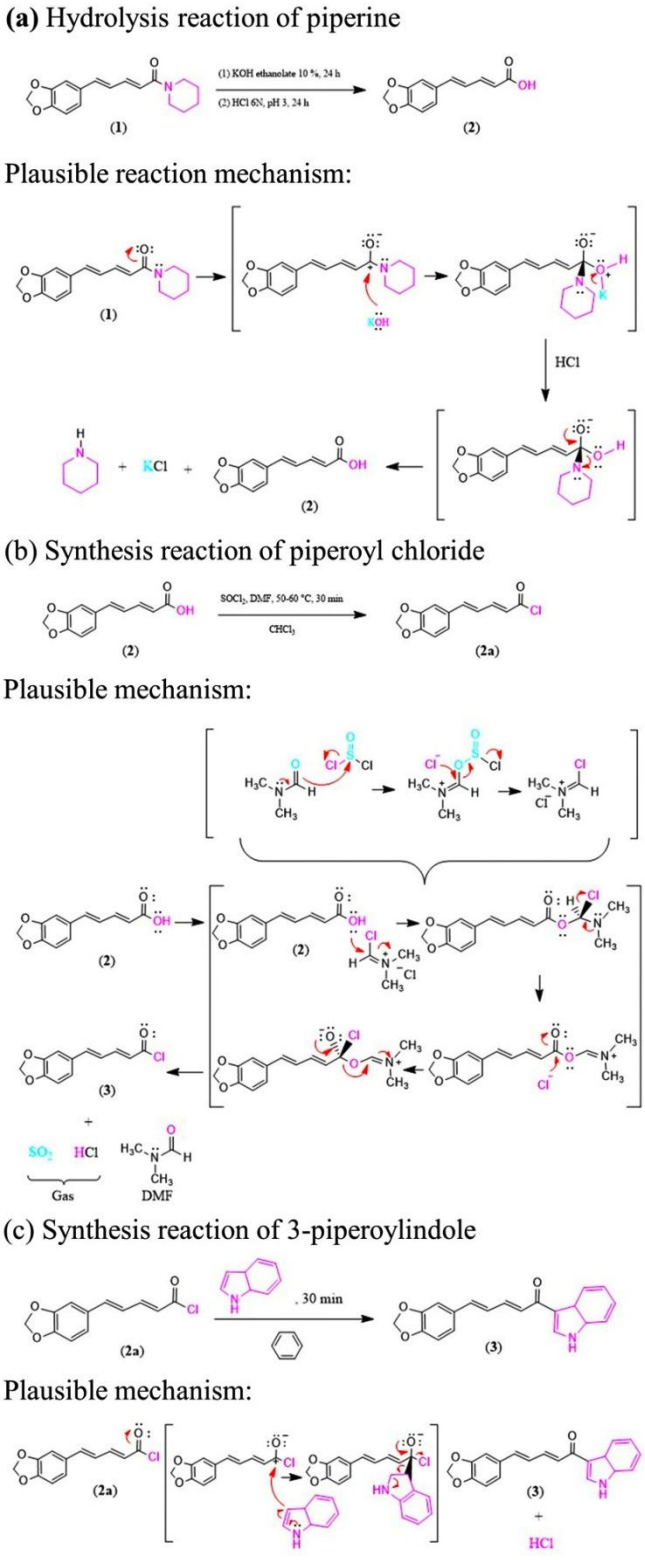

Figure 3 Plausible reactions and mechanisms for (a) hydrolysis of piperine, (b) synthesis of piperoyl chloride, and (c) synthesis of 3-piperoylindole.

***In silico* study: Molecular docking**

Table 1 displays the RMSD value of 1.382 Å for the native ligand to EGFR-TK (**Figure 4**) generated from the redocking using a specified grid box size. The RMSD value is the most commonly used parameter for evaluating the accuracy of docking geometry [25]. This value must be less than 2 to verify that the grid box size used in the docking method is acceptable [26].

Table 1 Redocking between EGFR-TK and native ligand.

Protein	PDB ID	Native ligand	Redocked RMSD (Å)
EGFR-TK	4HJO	Erlotinib	1.382

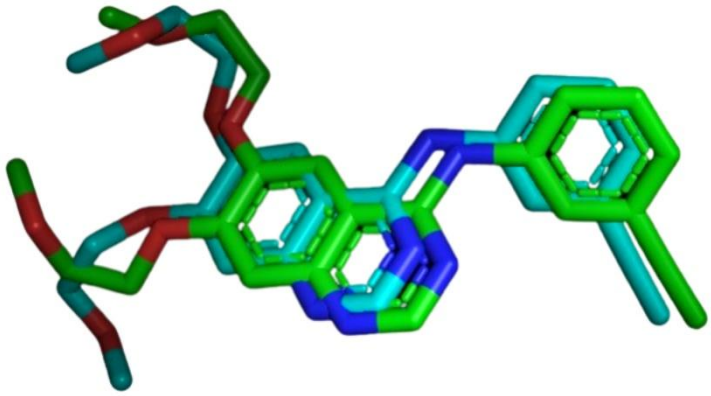

Figure 4 Visualization of redocking native ligand towards EGFR-TK.

Table 2 shows the values of the binding energies of 3-piperoylindole, with the value of −8.7 kcal/mol, observed in this study. This compound exhibited the lowest binding energies to EGFR-TK in comparison to erlotinib. EGFR-TK inhibitory activity is associated with compounds that have a lower binding energy and vice versa. This indicates that the inhibitory activity of this compound was considerably greater than that of erlotinib and that the interaction with EGFR-TK was more stable.

Table 2 Binding energies (kcal/mol) of the proposed compound towards EGFR-TK.

Compound	Binding energy (ΔG, kcal/mol)
3-piperoylindole	−8.7
Erlotinib	−7.7

In addition to binding energy, specific protein–ligand interactions that contribute to EGFR-TK inhibition were used as screening criteria. **Figure 3(a)** shows the 3D (left) and 2D (right) binding interactions of EGFR-TK with the native ligand erlotinib, while **Figure 3(b)** presents the same views for 3-piperoylindole. As detailed in **Table 3**, 3-piperoylindole forms two key hydrogen bonds with EGFR-TK: (1) The N-H group of the indole ring (proton donor) interacts with the carbonyl oxygen of Thr830 (acceptor). (2) The carbonyl group (C=O) of the ligand (electron pair acceptor) interacts with the amino group of Lys721 (proton donor).

Additionally, several hydrophobic and π-interactions are observed: (1) Val702, Leu820, and Ala719 engage in hydrophobic interactions with the heterocyclic aromatic ring and aliphatic chain of 3-piperoylindole. (2) Leu694 forms a π-σ interaction with the aromatic heterocyclic ring. (3) The indole ring further enhances hydrophobic contacts with Val702 and Ala719.

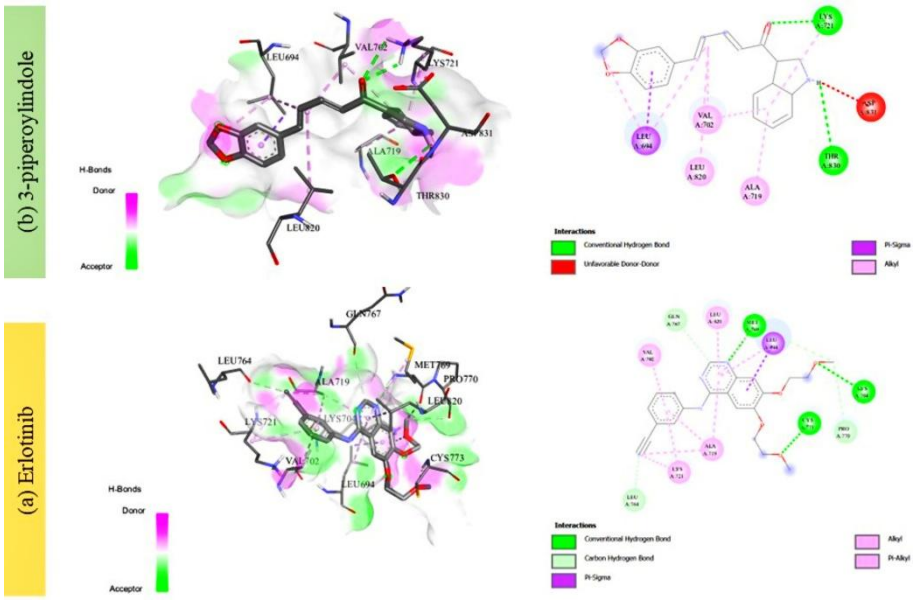

Figure 5 3D (left) and 2D (right) illustrations of (a) erlotinib and (b) 3-piperoylindole towards EGFR-TK.

We predict that the proposed ligand will only be able to partially establish hydrogen bonding interactions on hydrophilic groups, resulting in a mild inhibitory effect on this protein, as determined by the evaluation of binding energies and protein-ligand interactions. Consequently, we suggest the incorporation of hydrophilic substituents of 3-piperoylindole or piperine structures to facilitate the development of robust hydrogen bonding interactions.

Table 3 Interaction types of the proposed compound towards EGFR-TK.

Compound	Types of interaction		
	H-bond	**Hydrophobic**	**Others**
3-piperoylindole	Thr830 (2.93 Å); Lys721 (4.91 Å)	Val702; Leu820; Ala719	Pi-sigma: Leu694 (3.43 Å)
Erlotinib	Cys773 (2.06 Å); Lys704 (2.78 Å); Met769 (2.05 Å)	Val702; Leu820; Ala719; Lys721; Met769	Carbon H-bond: Leu764 (3.32 Å); Gln767 (3.78 Å); Pro770 (3.62 Å) Pi-sigma: Leu694 (3.40 Å)

Conclusions

In conclusion, we have successfully developed a method for the synthesis of 3-piperoylindole (3-PI) using piperoyl chloride as a key intermediate. Notably, this synthetic strategy can be applied to generate a variety of piperine derivatives derived from *Piper nigrum* Linn., a valuable natural source in medicinal chemistry. If yield or purity data are available, they could be included here to further support the robustness of the methodology. In addition, we conducted an *in silico* evaluation of 3-PI as a potential inhibitor of the EGFR-TK protein, using molecular docking analysis. The compound exhibited a binding energy of –8.7 kcal/mol, lower than that of the native ligand erlotinib (–7.7 kcal/mol), indicating a stronger affinity. Key interactions contributing to its binding include: (1) Hydrogen bonds with residues Thr830 and Lys721; (2) Hydrophobic interactions with Val702, Leu820, and

Ala719; (3) π-σ interaction with Leu694. These findings support further investigations of 3-piperoylindole as a promising EGFR-TK inhibitor. However, these *in silico* results require validation through *in vitro* and *in vivo* studies to confirm biological efficacy and specificity. Comparative analysis with other known EGFR inhibitors, such as gefitinib, may provide additional insight into its therapeutic potential evaluation.

Acknowledgements

This work was funded by the Higher Education Technology and Information (HETI) Project under contract number 238/UN26/HK.01.03/2024.

Declaration of Generative AI in Scientific Writing

During the preparation of this work the author(s) used DeepL and QuillBot tools in order to check the sentence structures and grammar. No content generation or data interpretation was performed by AI tools. After using this tool/service, the author(s) edited and reviewed the content as needed and take(s) full responsibility for the content of the publication.

CRediT author statement

Syaiful Bahri: Writing–original draft, Supervision, Conceptualization, Methodology, Formal analysis, Validation, Funding acquisition.

Devi Nur Annisa: Investigation, Methodology, Data curation, Resources.

Yuli Ambarwati: Writing–review & editing, Supervision, Formal analysis, Validation.

Lina Marlina: Writing–review & editing, Formal analysis, Validation, Data curation.

Sutiarno: Writing–review & editing, Formal analysis, Validation, Data curation.

Deana Wahyuningrum: Writing–review & editing, Formal analysis, Validation, Data curation.

Ganjar Andhulangi: Writing–review & editing, Software, Visualization, Formal analysis, Data curation, Validation.

References

[1] RL Siegel, TB Kratzer, AN Giaquinto, H Sung and A Jemal. Cancer statistics, 2025. *CA: A Cancer Journal for Clinicians* 2025; **75(1)**, 10-45.

[2] A Sharma, S Jasrotia and A Kumar. Effects of chemotherapy on the immune system: Implications for cancer treatment and patient outcomes. *Naunyn-Schmiedeberg's Archives of Pharmacology* 2023; **397(5)**, 2551-2566.

[3] J Rueff and AS Rodrigues. *Cancer drug resistance: A brief overview from a genetic viewpoint. In*: J Rueff and AS Rodrigues (Eds.). Methods in Molecular Biology. Humana Press, New York, 2016.

[4] M Habban Akhter, N Sateesh Madhav and J Ahmad. Epidermal growth factor receptor based active targeting: A paradigm shift towards advance tumor therapy. *Artificial Cells, Nanomedicine, and Biotechnology* 2018; **46(2)**, 1188-1198.

[5] E Kovacs, JA Zorn, Y Huang, T Barros and J Kuriyan. A structural perspective on the regulation of the epidermal growth factor receptor. *Annual Review of Biochemistry* 2015; **84(1)**, 739-764.

[6] JJ Laskin and AB Sandler. Epidermal growth factor receptor: A promising target in solid tumours. *Cancer Treatment Reviews* 2004; **30(1)**, 1-17.

[7] RM Sylva and SI Ahmed. Targeted therapies in cancer. *Surgery* 2024; **42(3)**, 150-155.

[8] C Schettino, MA Bareschino, P Maione, A Rossi, F Ciardiello and C Gridelli. Small molecule epidermal growth factor receptor (EGFR) tyrosine kinase inhibitors in non-small cell lung cancer treatment. *Current Cancer Therapy Reviews* 2007; **3(4)**, 226-235.

[9] XL Huang, MI Khan, J Wang, R Ali, SW Ali, QA Zahra, A Kazmi, A Lolai, YL Huang, A Hussain, M Bilal and F Li. Role of receptor tyrosine kinases mediated signal transduction pathways in tumor growth and angiogenesis - New insight and futuristic vision *International Journal of Biological Macromolecules* 2021; **180**, 739-752.

[10] CJ Tsai and R Nussinov. Emerging allosteric mechanism of EGFR activation in physiological and pathological contexts. *Biophysical Journal* 2019; **117(1)**, 5-13.

[11] DA Sabbah, R Hajjo and K Sweidan. Review on epidermal growth factor receptor (EGFR) structure, signaling pathways, interactions, and recent updates of EGFR inhibitors. *Current Topics in Medicinal Chemistry* 2020; **20(10)**, 815-834.

[12] AK Kashyap and SK Dubey. *Molecular mechanisms in cancer development. In*: B Jain and S Pandey (Eds.). Understanding cancer. Academic Press, New York, 2022, p. 79-90.

[13] R Damare, K Engle and G Kumar. Targeting epidermal growth factor receptor and its downstream signaling pathways by natural products: A mechanistic insight. *Phytotherapy Research* 2024; **38(5)**, 2406-2447.

[14] H Takooree, MZ Aumeeruddy, KRR Rengasamy, KN Venugopala, R Jeewon, G Zengin and MF Mahomoodally. A systematic review on black pepper (*Piper nigrum* L.): From folk uses to pharmacological applications. *Critical Reviews in Food Science and Nutrition* 2019; **59(S1)**, S210-S243.

[15] PV Dludla, I Cirilli, F Marcheggiani, S Silvestri, P Orlando, N Muvhulawa, MT Moetlediwa, BB Nkambule, SE Mazibuko-Mbeje, N Hlengwa, S Hanser, D Ndwandwe, JL Marnewick, AK Basson and L Tiano. Bioactive properties, bioavailability profiles, and clinical evidence of the potential benefits of black pepper (*Piper nigrum*) and red pepper (*Capsicum annum*) against diverse metabolic complications. *Molecules* 2023; **28(18)**, 6569.

[16] DR Anandh and D Priya. Review on the pharmacological activities of black pepper. *Journal of Natural Remedies* 2024; **24(3)**, 441-451.

[17] Y Liu, VR Yadev, BB Aggarwal and MG Nair. Inhibitory effects of black pepper (*Piper Nigrum*) extracts and compounds on human tumor cell proliferation, cyclooxygenase enzymes, lipid peroxidation and nuclear transcription factor-kappa-B. *Natural Product Communications* 2010; **5(8)**, 1253-1257.

[18] PM Paarakh, DC Sreeram and SPS Ganapathy. *In vitro* cytotoxic and *in silico* activity of piperine isolated from *Piper nigrum* fruits Linn. *In Silico Pharmacology* 2015; **3(1)**, 9.

[19] S Bahri, Y Ambarwati, M Iqbal and AA Baihaqy. Synthesis 4-piperoilmorpholine from piperine. *Journal of Physics: Conference Series* 2019; **1338(1)**, 012010.

[20] NK Singh, P Kumar, DK Gupta, S Singh, and VK Singh. UV-spectrophotometric method development for estimation of piperine in Chitrakadi Vati. *Der Pharmacia Lettre* 2011; **3(3)**, 178-182.

[21] L Gorgani, M Mohammadi, GD Najafpour and M Nikzad. Sequential microwave-ultrasound-assisted extraction for isolation of piperine from black pepper (*Piper Nigrum* L.). *Food and Bioprocess Technology* 2017; **10(12)**, 2199-2207.

[22] A Yasir, S Ishtiaq, M Jahangir, M Ajaib, U Salar and KM Khan. Biology-Oriented Synthesis (BIOS) of piperine derivatives and their comparative analgesic and antiinflammatory activities. *Medicinal Chemistry* 2018; **14(3)**, 269-280.

[23] P Choochana, J Moungjaroen, N Jongkon, W Gritsanapan and P Tangyuenyongwatana. Development of piperic acid derivatives from *Piper nigrum* as UV protection agents. *Pharmaceutical Biology* 2014; **53(4)**, 477-482.

[24] Z Zarai, E Boujelbene, NB Salem, Y Gargouri and A Sayari. Antioxidant and antimicrobial activities of various solvent extracts, piperine and piperic acid from *Piper nigrum*. *LWT - Food Science and Technology* 2013; **50(2)**, 634-641.

[25] DM Aziz, JR Hama and SM Alam. Synthesising a novel derivative of piperine from black pepper (*Piper Nigrum* L.). *Journal of Food Measurement and Characterization* 2015; **9(3)**, 324-331.

[26] I Kufareva and R Abagyan. *Methods of protein structure comparison. In*: A Orry and R Abagyan (Eds.). Methods in molecular biology. Humana Press, New Jersey, United States, 2011, p. 231-257.

[27] M Sandor, R Kiss and GM Keserű. Virtual fragment docking by glide: A validation study on 190 protein-fragment complexes. *Journal of Chemical Information and Modeling* 2010; **50(6)**, 1165-1172.